Engineering Failure Analysis 153 (2023) 107543

Contents lists available at ScienceDirect

Engineering Failure Analysis

journal homepage: www.elsevier.com/locate/engfailanal

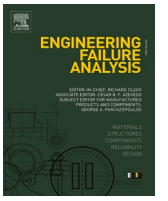

# Failure analysis of corroded heat exchanger CuNi tubes from a geothermal plant

Joseph B. Morake [a,*], James M. Mutua [a], Martin M. Ruthandi [a], Eyitayo O. Olakanmi [b,c,d], Annelize Botes [e]

[a] School of Mechanical Manufacturing and Materials Engineering, Jomo Kenyatta University of Agriculture and Technology (JKUAT), Nairobi, Kenya
[b] Department of Mechanical Energy and Industrial Engineering, Botswana International University of Science and Technology (BIUST), Palapye, Botswana
[c] UNESCO Chair on Sustainable Manufacturing & Innovation Technologies (UCoSMIT), Botswana International University of Science and Technology, Palapye, Botswana
[d] Advanced Manufacturing & Engineering Education (AMEE) Research Group, Botswana International University of Science and Technology, Palapye, Botswana
[e] Department of Mechanical Engineering, Nelson Mandela University, Port Elizabeth, South Africa

ARTICLE INFO

*Keywords:*
Heat exchanger
Cupronickel
Hydrogen embrittlement
Sulfide stress cracking
Tube wear

ABSTRACT

This study examined the premature failure of cupronickel (CuNi10Fe) tubes in a shell-and-tube heat exchanger after five months of service. An investigation to identify the root cause of the tube burst was carried out using macroscopic and microscopic inspection, chemical analysis, and mechanical analysis. The optical microscopy (OM) and scanning electron microscopy (SEM) evaluation revealed crack propagation characterized by pits and inclusions at the tube surface. This was due to the diffusion of hydrogen ions into the material from the hydrogen sulfide ($H_2S$) rich geothermal environment. Furthermore, high tensile residual stresses of 172 MPa were recorded in the failed tube, leading to stress cracking in hydrogen-containing material. Additionally, the high sulfide content in corroded water and condensate samples suggests that the leading cause of tube rupture was through hydrogen embrittlement and sulfide stress cracking mechanism in the presence of hydrogen sulfide. Therefore, the use of laser cladding to protect tubes using functionally graded materials is recommended to mitigate degradation in aggressive environments, through careful material selection and additional water treatment to eliminate the contaminants.

## 1. Introduction

Heat exchangers are crucial devices in process industries for transferring or dissipating heat from one medium to another [1]. Heat exchanger tubes fail frequently during heat transfer due to material degradation. Corrosion degradation failures such as corrosion erosion, corrosion cracking, and corrosion fatigue are some of the most dominant failure mechanisms aggravated by corrosive media, cyclic loads, high pressures, and high temperatures [2]. Copper and its alloys have found application in the manufacture of boiler tubes, due to their high thermal conductivity and better formability [3]. Meanwhile, most tubes made of copper alloy have limited

* Corresponding author.
*E-mail address:* josephblmorake@gmail.com (J.B. Morake).

https://doi.org/10.1016/j.engfailanal.2023.107543
Received 5 June 2023; Received in revised form 24 July 2023; Accepted 13 August 2023
Available online 18 August 2023

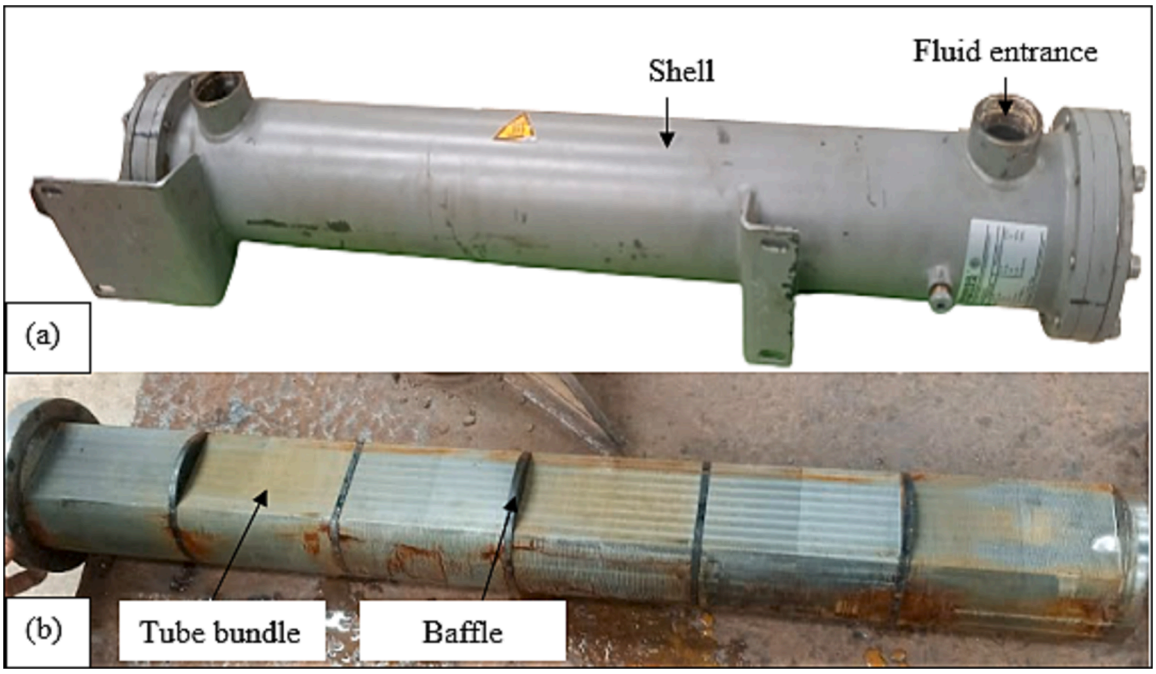


**Fig. 1.** View of the failed shell-and-tube heat exchanger, (a) general view of the exchanger and (b) internal assembly of the tube bundle.

resilience in hostile environments, implying the need for surface modification using resilient materials that can withstand wear erosion and stress cracking during operation at elevated temperatures and high pressures [4,5]. Surface modification of copper alloy tubes can mitigate the degradation aggravated by the presence of both tensile residual stresses and corrosive media/agents [6].

Researchers have investigated numerous heat exchanger copper tube failures encountered in several process industries. Kuznicka [7] investigated the root cause of failure in an industrial cooling system's shell and tube heat exchanger. The exchanger using copper tubes was found to have failed because of erosion-corrosion. The authors attributed the failure to the high chloride content of 821 mg/l in the water. This resulted in pit formation on the surface of the tube by destabilizing the protective layer of cuprous oxide, which shows that chloride can gradually degrade the tube's inner surface over time and promote the formation of pitting corrosion. Lachowicz [8] studied the cause of formicary corrosion in heat exchangers made of copper tubes and the results showed that the corrosion products developed within the tube on the inside walls and diffused to the outer tube wall. The results revealed that this caused crack formation due to local stresses, leading to crack propagation in phosphorus-rich areas of the tube material. This demonstrates that copper tubes are prone to stress corrosion cracking and pit formation when operating in aggressive environments, leading to reduced heat transfer and premature failures.

Mousavian et al. [9] investigated the failure of heat exchanger tubes made of copper. The formation and deposits of corrosive products on the tube wall were found to cause flow stoppage and tube clogging. Consequently, this reduced the heat transfer and caused tube failure due to severe expansion strains. In some related work, Wang et al. [10] examined the cause of cracking failure in AISI grade 304 stainless steel heat exchanger tubes after eight months of use. They affirmed the presence of copper ions, high temperature, and mechanical stresses yielded to inter and transgranular cracks that failed. The authors recommended the use of grade 2205 duplex stainless steel instead of grade SS304, which they examined and never failed in the same operating conditions. This indicates that materials respond differently to various corrosive media. It also implies that mechanical stresses can alter the microstructure of a part, reducing its fracture toughness and increasing the risk of fatigue and corrosion cracking. Failure analysis of heat exchangers plays a significant role in determining the cause and mechanism of crack propagation to avoid future occurrences of the same problem. In this study, the failure analysis was performed on a shell-and-tube heat exchanger to determine the cause of tube rupture.

The heat exchanger was used in a 165 MW geothermal power plant and failed prematurely after five months of usage. This resulted in significant maintenance expenses for tube replacement and eventual overhaul of the heat exchanger. Additionally, this disrupted the power plant output capacity. The heat exchanger design consists of a copper-nickel tube bundle wrapped in a tube sheet, responsible for compressing air through a thermal heat transfer process that uses water flowing at high pressure (7.7 bar) and temperature (144 °C), as shown in Fig. 1. The geothermal environment contains gaseous compounds in the form of hydrogen sulfide ($H_2S$), a noxious corrosive and toxic gas with a repugnant smell.

The exchanger was part of a four-stage compression system in the condenser unit. Its main function is to cool the water from 144 °C to 27 °C while operating at a pressure of 2.0 bars. Stacked stainless steel plates firmly held the tubes together to withstand unwanted tube vibrations and to increase the heat transfer surface area. Additionally, the shell side contained dry air for efficient heat transfer, and the operation schematic of the failed heat exchanger conditions is shown in Fig. 2.

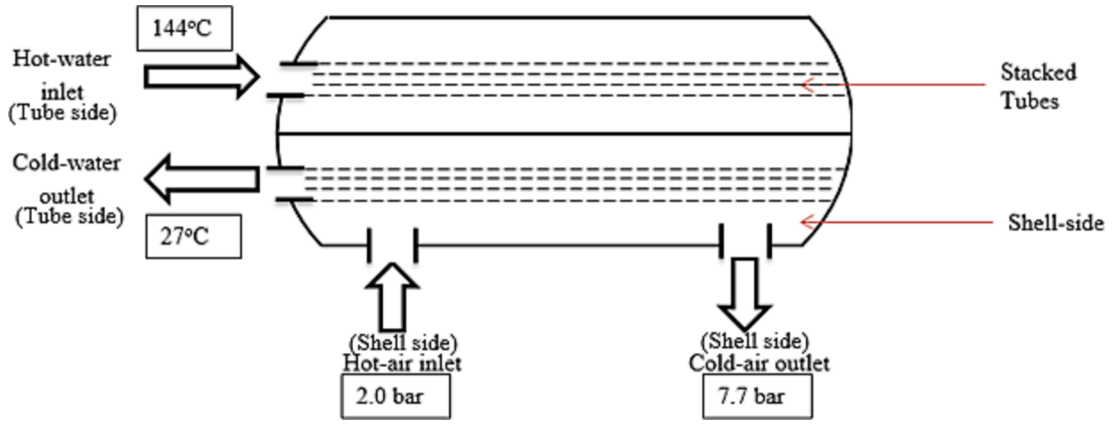


**Fig. 2.** Schematic representation of the shell and tube heat exchanger.

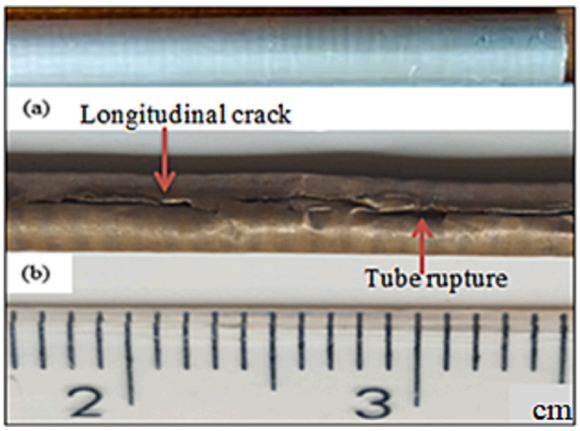


**Fig. 3.** Investigated heat exchanger tubes (a) intact tube, T1 (b) failed tube, T2.

The heat exchanger tubes underwent material degradation and tube failure due to adverse environmental factors. This circumstance resulted in tube leaks, pressure drops, and tube bursts, which caused fluid mixing. Since each heat exchanger's operating environment has different operational parameters, the failure analysis is conducted to identify the primary factor that led to the tube burst. Because of this, the failure mechanisms of the heat exchangers utilized at the Olkaria geothermal power plant will differ from those generally described in the literature, and the solutions recommended to reduce the failure will be specially designed for these power plant conditions. The aim is to lower the number of heat exchanger failures.

## 2. Materials and methods

The experimental method was carried out using visual inspection, chemical analysis, microstructural observation, and mechanical tests, to identify the mechanism of tube failure.

### *2.1. Visual inspection of the tube samples*

Two heat exchanger tubes were extracted for examination based on functionality. The first tube was identified as the intact tube and used as the control tube (sample T1), while the second tube was identified as the ruptured/failed tube (sample T2), as shown in Fig. 3. The failed heat exchanger tubes were visually observed to identify failure characteristics that can be seen with eyes.

### *2.2. Chemical analysis of the water*

The chemical composition of the condensate that is used for cooling in the heat exchanger chambers and the corroded water obtained from the failed heat exchanger tubes were tested using a UV spectrophotometer (Shimadzu Cooperation, Japan) for compounds. The turbidity meter for the Nephelometric Turbidity unit (NTU) test was employed to measure the cloudiness of the water. Additionally, the oven drying method was used to quantify the total dissolved solids (TDS), while the Flame emission

**Table 2**
Chemical composition of the water circulating in the heat exchanger.

| Elements | Steam condensate | Corroded water |
|---|---|---|
| Total dissolved solids, TDS (ppm) | 218 | 1833 |
| pH level | 6.89 | 8.10 |
| Turbidity, NTU | 4.6 | 430.8 |
| Conductivity (μS/cm) | 340.10 | 2860 |
| Chloride ions, $Cl^-$ (ppm) | 8.25 | 23.75 |
| Total Phosphates, $PO_4$ (ppm) | 0.02 | 0.045 |
| Sulphates, $SO_4^{2-}$ (ppm) | 1159.59 | 1248.06 |
| Ammonia nitrogen, $NH_4$ (ppm) | 47.1 | 258.61 |
| Sulfides (ppm) | 49.5 | 126.27 |
| Nitrates, $NO_3^-$ (ppm) | 2.36 | 26.8 |
| Magnesium, Mg | 0.98 | 1.55 |
| Sodium, Na | 6.08 | 11.3 |
| Potassium, K | 0.94 | 3.21 |
| Zinc, Zn | 0.02 | 0.03 |
| Iron, Fe | 0.01 | 1.4 |
| Calcium, Ca | 0.22 | 2.16 |

**Table 1**
Summary of the sample information and the measuring conditions.

| Description | Value |
|---|---|
| Sample distance(Monitor) | 51.00 mm |
| X-ray tube voltage | 30.00 kV |
| Tilt angle | 35.0 deg |
| Peak analysis method | Fitting Lorentz |
| Total measurement count | 50 |
| X-ray irradiation time(Max) | 50 sec |

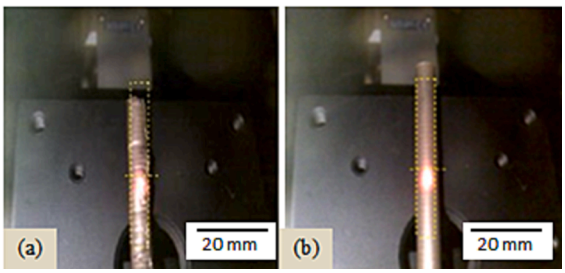


**Fig. 4.** Sample positioning for residual stress measurements (a) failed tube and (b) intact tube.

spectrophotometer (FES) and Atomic absorption spectroscopy (AAS) methods were used to measure metallic ions. The hydrogen sulphite in the geothermal environment was examined using lead acetate test paper, whilst the sulphides in the corroded and condensate water were tested using the iodometric method. The paper was quickly immersed in water, and the darkening of the paper indicates that there is $H_2S$ in the water.

### *2.3. Microstructural investigation of the failure samples*

#### *2.3.1. Sample preparation*

Sample T1 and T2 heat exchanger tubes were sectioned along the cross-section using Struers Labotom-15 cutting machine. To observe the internal corrosion products in the failed tube, the third sample was sectioned circumferentially for analysis. Samples were mounted on polymer resin using a mounting Press, and then ground using abrasive grit of sizes 320, 500, and 1200. Thereafter, the samples were polished using MD Largo cloth and 9 μm diamond suspension to obtain a mirror finish. For SEM analysis, the sample was gold coated to ensure surface conductivity.

#### *2.3.2. Optical microscopic observation of samples*

Olympus optical microscope was used to analyse samples T1 and T2 to identify the internal surface defects. This include observing the surface cracks and pits to ascertain the root cause of failure.

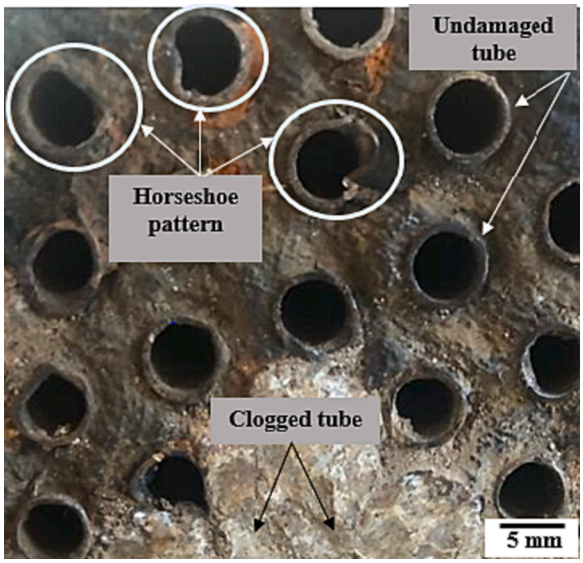


**Fig. 5.** Top view of the failed heat exchanger tube bundle.

*2.3.3. Scanning electron microscope of samples (including EDS)*

The JSM-7100F scanning electron microscope equipped with energy-dispersive spectroscopy (SEM-EDS) was used to identify failure features at a higher magnification. The focus was to identify the origin of the failure, and crack propagation, and quantify the defects (cracks, pits, and inclusions) present. Horiba XGT-9000 X-ray Fluorescence analyzer (Kyoto, Japan) was used to determine the oxides and elements in the corrosion residues. The results were also validated using SEM-EDS.

*2.4. Residual stress measurements*

Residual stresses were measured using the μ-X360s Portable X-ray Residual Stress Analyser (Pulstec Ltd, Japan). Table 1 summarises the parameters adopted for the residual stress measurements. The residual stresses were measured for sample T1 and T2. Residual stresses were measured at the tube surface along the tube's circumferential direction, see Fig. 4.

## 3. Results and discussion

*3.1. Visual examination and mechanical analysis*

The results of the visual inspection are interpreted in light of the mechanical study to clarify the mechanism by which the visible failure features emerged. Fig. 5 shows the cross-section of the virtually inspected stacked exchanger tubes. White blockage media introduced to the exchanger by the Olkaria Company were observed at the tube end (see Fig. 5), and found to correspond to the blocked dysfunctional tubes. On the contrary, the tubes at the outer region of the bore appeared to be in good shape and to be working properly. To confirm this, the pressure was blown through the pipe and dysfunctional tubes were identified by leakage sound. This may indicate that corrosion predominantly took place at the centre because cracking was primarily concentrated at the tube bundle's centre and stretched along the tube's longitudinal direction, as illustrated in Fig. 3b. This could also be due to the shell side turbulent pressure concentrated at the centre, implying that the exchanger failure emanated from the centre tubes due to high stress concentrated regions.

The assertion on the occurrence of high-stress concentrations at the tubes located at the centre of the heat exchanger is corroborated by the outcomes of mechanical analysis of samples T1 and T2, see Fig. 6. It is clear from Fig. 6 that the failed tube (sample T2) exhibited high levels of tensile residual stresses with a value of positive 172 MPa. The presence of residual stress reduces the material fracture toughness, rendering the tube more likely to experience failure through crack propagation. Compressive residual stresses, which are not harmful nor speed up tube deterioration, were detected for sample 1. This is owing to the reason that compressive residual stresses on tube surfaces are suggested to prevent the movement or diffusion of hydrogen atoms because they increase the material's hardness. By enhancing the integrity of the material, the diffusion and concentration of hydrogen concentration in the material is reduced, and the prevalence of hydrogen stress cracking is controlled. Meanwhile, the concentration of hydrogen invasion and ultimate cracking is exacerbated by tensile residual stresses since they suppress fatigue strength [11,12]. Therefore, it can be inferred that the material quality of sample T1 was still in its integrity with less hydrogen concentration, thereby reducing the likelihood of hydrogen induced cracking.

The peak profile of the intact tube had a low level of stress intensity, which affects the rate at which cracks propagate, and was distinguished by a thin blue lining to indicate decreased stress intensity (Fig. 6a). Fig. 6 (a) shows the residual stress values for sample T1 (Intact tube) and sample T2 (failed tube), which were auto-generated by the residual stress analysing machine. It is evident from

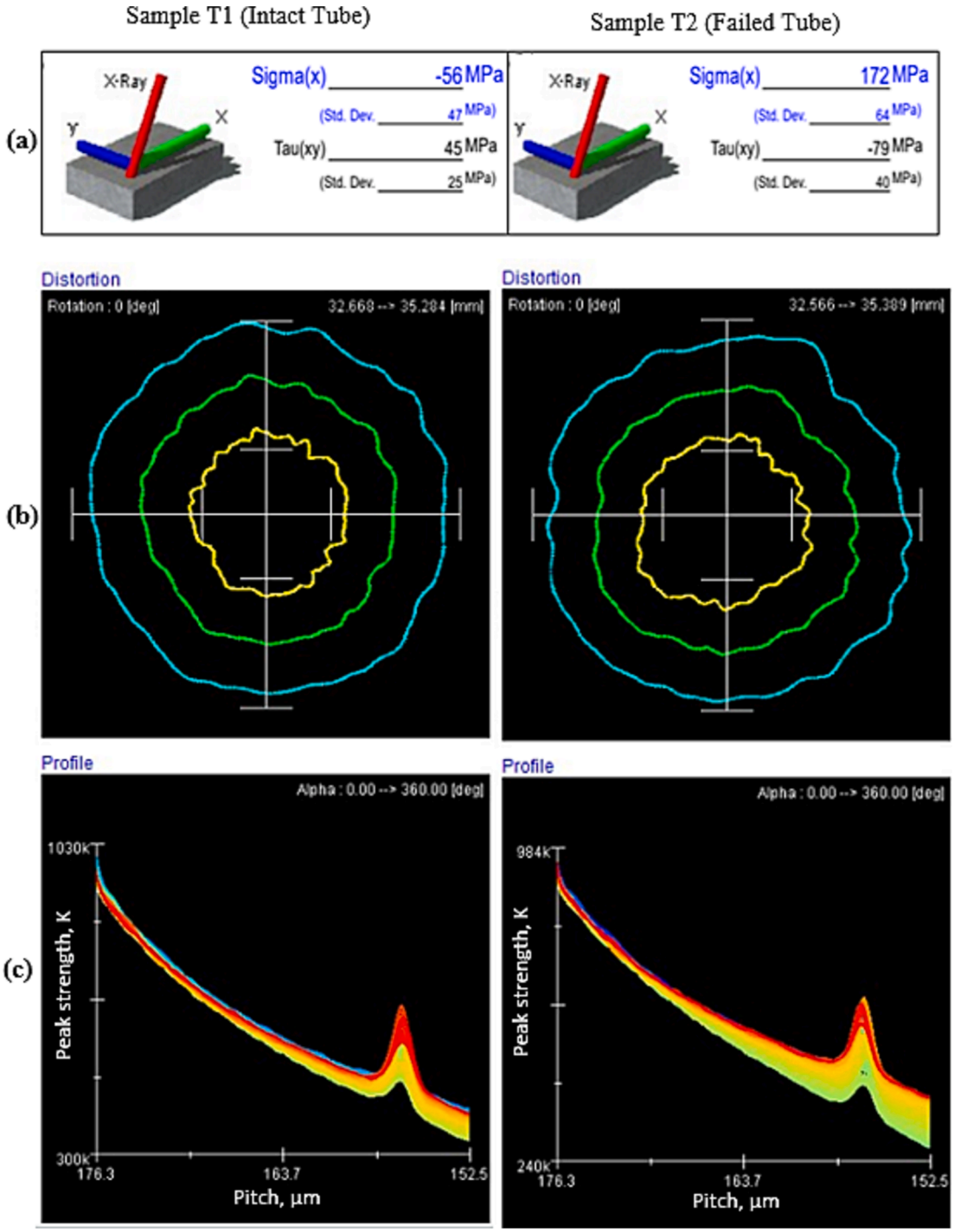


**Fig. 6.** Measurement of internal residual stresses at tube surface compared for sample T1 and T2 (a) stress values (b) distortion (c) residual stress profile.

Fig. 6 (a) that the failed tube has tensile residual stresses of positive 172 MPa, while the intact tube has compressive residual stresses of negative 56 MPa. The failed tube's distortion (Fig. 6b) is also higher than the undamaged tube's due to high-stress concentrations, measuring 2.823 mm, which supports the explanation behind the expanded region of the failed tube observed in Fig. 4b. Furthermore, the intact tube is more accurately depicted in Fig. 6b with a circumference that is close to circular, as opposed to the failed tube Fig. 6b with a more distorted shape. In contrast, the failed tube's peak profile in Fig. 6c featured a thick peak profile with a yellow–red line signifying high-stress intensity.

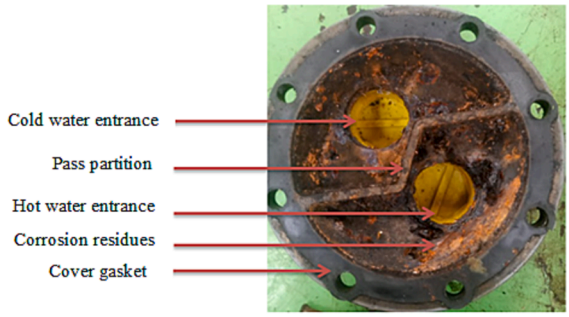


**Fig. 7.** Corroded heat exchanger cover showing brownish-to-red corrosion products with black layers.

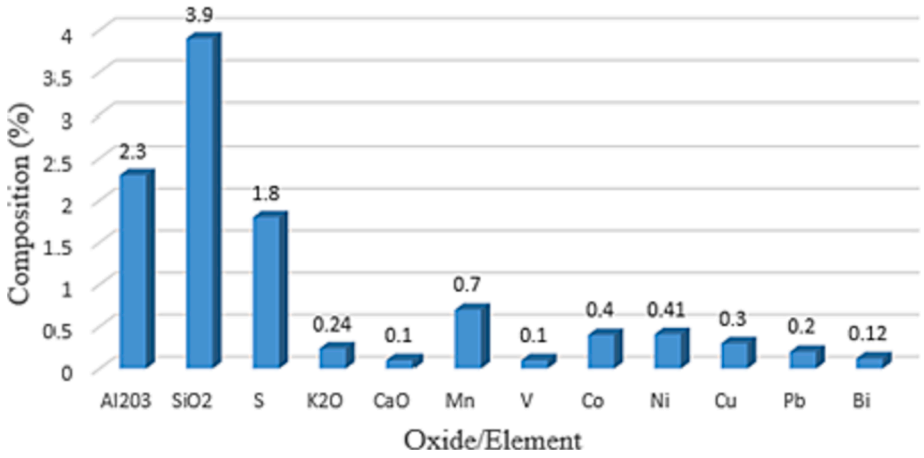


**Fig. 8.** Elemental distribution and composition of corrosion residue.

A similar observation was reached by Usman & Khan [13] when investigating ASTM A213 grade T11 heat exchanger tubes. They found that stresses induced by cyclic temperature swings caused tube cracking because of thermal fatigue, which indicates that stresses influence the material's resistance to degradation. Therefore, it can be argued that the CuNi experienced high-stress levels beyond its yield point, leading to cracking, which in the presence of high sulphate content became sulphide-induced stress corrosion cracking. This was also seen in the work of Miyamoto et al. [14], who investigated the stress corrosion cracking of pure copper and found that it was caused by the accumulation of residual stress and strain at grain boundaries. In a related study, Xu et al. [15] conducted a failure analysis on stainless steel heat exchanger tubes and concluded that SCC due to residual tensile stresses was the cause of premature failure, showing that tensile residual stresses can exacerbate the SCC failure mechanism.

Furthermore, horseshoe patterns could be seen at the tube entrance, implying the occurrence of erosion. The horse shoe pattern are categorized by an extended circular arc with a narrow bottom view, just like typical shoeing of horse's (see Fig. 5). This suggests that the tube took on a shape resembling a normal horse shoe foot print as a result of distortion spurred by high fluid pressure. Also, the high-pressure water turbulence encountered when water divides from the large pipe into the smaller diameter tubes at high velocities resulted in tube thinning and dislocation aggravated by abrasive particles in the fluid. Visual observations of the shell and tube heat exchanger cover also showed the presence of brownish-to-red corrosion products with black layers, as indicated in Fig. 7. However, the gasket did not fail as it was intact with no signs of cracking or dislocation. According to Chandra et al. [16], the reddish-brown substance observed is a cuprous oxide ($Cu_2O$) that is formed when the copper reacts with air, to act as a protective film against degradation. In this case, it possibly eroded and got washed away in the presence of corrosive products formed over chemical reactions. Migration of corrosion products can take place in CuNi tubes, as seen in the work of Mousavian et al. [9] when corrosion products moved from the tube front-end into heat exchanger copper tubes.

### *3.2. Chemical analysis of water samples and corrosion residue*

Table 2 gives a summary of the recorded values obtained for both industrial water (W1) and steam condensate (W2). The water analysis revealed that both samples W1 and W2 contain high sulfides content, which has been reported to be the main corrosion-degrading agent for sulphide stress cracking of pipelines [17,18]. Studies have shown that sulphides, even at low concentration (<10 ppm), can be lethal and cause corrosion of industrial plant equipment [19]. However, it is seen from Table 2 that sample W2 contain higher content sulphates relative to W1. This is due to the chemical reactions that led to the formation of corrosion products, as

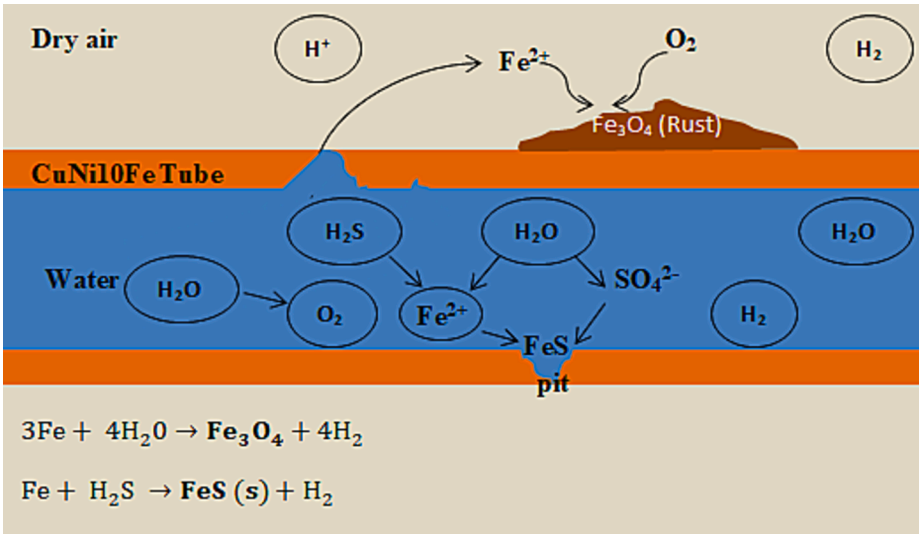


**Fig. 9.** Schematic illustration of the corrosion process of CuNi10Fe.

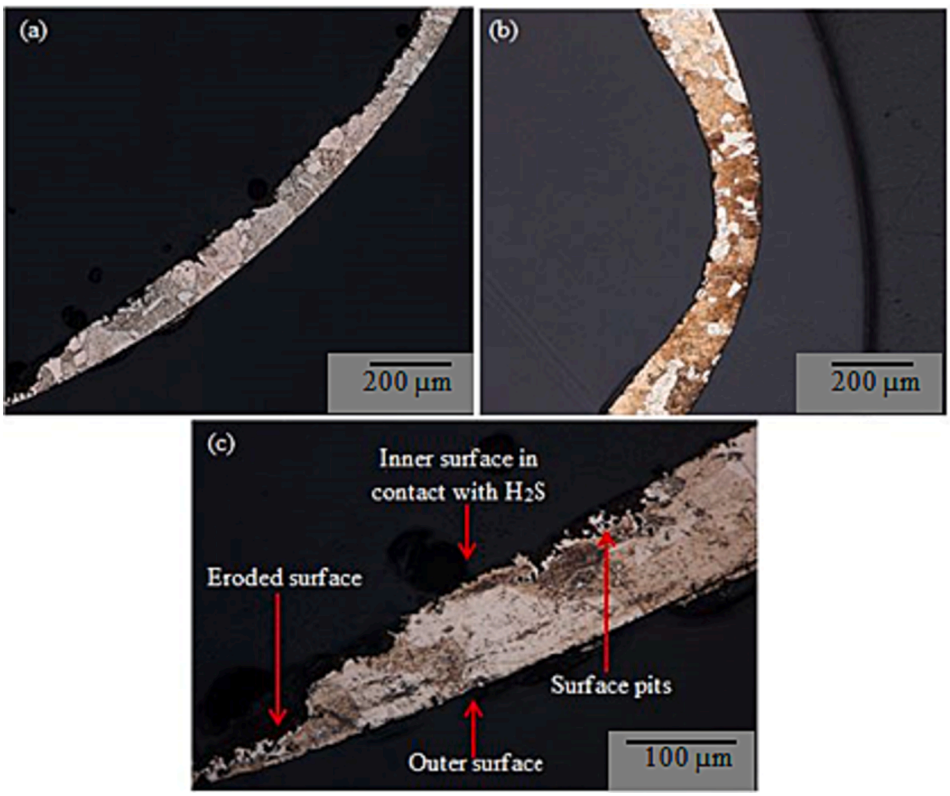


**Fig. 10.** Micrographs of heat exchanger tubes (a) failed tube with surface defects (b) intact heat exchanger tube with less surface distortion (c) surface cracks pits growing from the inside.

can be seen with an increase in totally dissolved solids and conductivity. Because of this, sulphates are believed to have caused stress corrosion cracking. Generally, when a material under stress (or residual stress) is exposed to sulphur-induced contaminants or sulphates, it becomes susceptible to sulphide stress corrosion cracking. Tuck & Emea [20] posited that, while cupronickel is not frequently prone to sulphide stress corrosion cracking in fluids containing low sulphate concentrations, it can experience catastrophic pipe failure when the sulphate concentration is high (>100 ppm). Based on this argument, it is certain the high sulphate content in the industrial water contributed to crack propagation. On the other hand, excess chloride content is also reported to contribute to stress corrosion

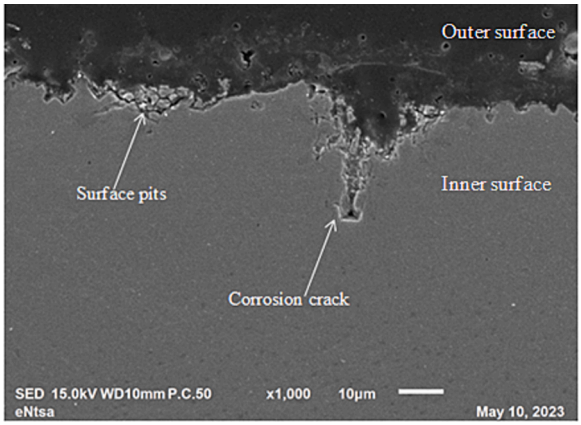


**Fig. 11.** SEM morphology of sulfide-induced degradation at the tube lining.

cracking. Wang et al. [10] revealed that copper can be oxidized in a reaction with water and chloride ions, causing the replacement of the $Cu_2O$ oxide layer by chloride ions, and eventually leading to pit formation and crack growth. Corte et al. [21] established that the high chloride content contained in the cooling water initiated cracks leading to SCC failure. Therefore, it is highly probable that the chloride ions in the present study contributed to pit formation.

### 3.3. X-ray fluorescence analysis

The corrosion residues from the tube bundle and shell cover were analysed using Brukers XRF machine for elemental analysis. The elements greater than 1% picked in XRF analysis were iron oxide ($Fe_3O_4$), silicon dioxide ($SiO_2$), aluminium oxide ($Al_2O_3$), and sulphur, respectively. The compounds discovered in the residues are represented graphically in Fig. 8 except for ($Fe_3O_4$), which was present in excess and balanced the composition.

The pit formation of CuNi pipes due to iron oxidation led to the depletion of iron in the presence of $H_2S$, which gave room for the diffusion of hydrogen ions and susceptibility of embrittlement, resulting in hydrogen-induced cracking in sulphide concentrated environment. This is evidenced by the black and orange-brown colour of the corrosion residues that were examined, referred to as iron oxide, and commonly known as rust. Furthermore, the presence of sulphur was observed to be excessive. It can lead to sulfidation that results in sulphide or sulphate formation due to the compounds triggered by the presence of Fe and Ni, which are significant contributions and responsible for acceleration corrosion in copper-nickel tubes and cracking. Thus, the presence of iron in the corroded powder could mean iron was oxidized at the anode to its ferrous form and reacted with steam containing hydrogen sulphide at the cathode, forming an unprotective iron oxide ($Fe_3O_4$). Fig. 9 also shows the degrading mechanism in the presence of magnetite, which is a product of iron oxide, is formed on the steam side of the boiler tubes under high pressure and high temperature in a humid environment.

### 3.4. Optical microscopy analysis

The optical micrograph in Fig. 10 shows the microstructure of the failed tube. Thinning of the tube lining characterized by surface pits can be seen along the surface. The presence of a grooved surface could mean the penetration of hydrogen into the material when it comes into contact with $H_2S$. In the examined case, it is apparent that the direct contact of the cupronickel surface with degrading impurities particularly sulfides, resulted in perforation of the tube surface.

According to Yang et al. [23], sulphur segregation can damage grain boundaries and cause cracking corrosion. This is explained by the fact that vanadium and sulphur together can produce salts, which can cause sedimentation and pit development. Pits crack when they experience tensile tension. On the contrary, the wall thickness of the intact tube is seen to be compact with cracks and pits, which could be the reason that the tubes did not rupture, leak, or fail during service. Meanwhile, the intact tube also experienced erosion wear since the circumferential thickness is not uniform. This suggests the first mechanism of degradation was erosion-wear of the tube wall, followed by pit formation and crack due to depletion of the protective layer.

### 3.5. Scanning electron microscopic and EDS analysis

Scanning electron microscopic (SEM) analysis was employed in this study to identify the microstructure, morphology, point of origin, orientation, and growth of the cracks. EDS analysis helped to determine the chemical composition of inclusions and corrosion residues present in the corroded exchanger tubes. Fig. 11 shows the degradation of the failed tube material with surface pits visible at the outer edge of the tube wall. Additionally, a primary crack branch can be seen propagating from the tube surface, taking the form of SCC caused by a sulphide-rich medium. This could mean some chemical reactions took place and led to an attack on the tube lining.

(a)

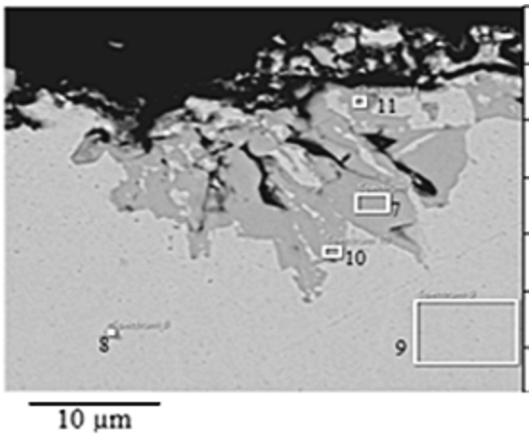


(b)

| El. | 7 | 8 | 9 | 10 | 11 |
|---|---|---|---|---|---|
| O | 10.24 | 9.38 | 0.00 | 8.79 | 10.51 |
| Mn | 0.00 | 0.00 | 0.89 | 0.35 | 0.00 |
| Fe | 0.45 | 0.00 | 1.50 | 0.48 | 0.62 |
| Ni | 0.95 | 1.40 | 9.36 | 3.30 | 0.87 |
| Cu | 88.36 | 89.22 | 88.25 | 87.08 | 88.00 |
| Total | 100.0 | 100.0 | 100.0 | 100.0 | 100.0 |

(c)

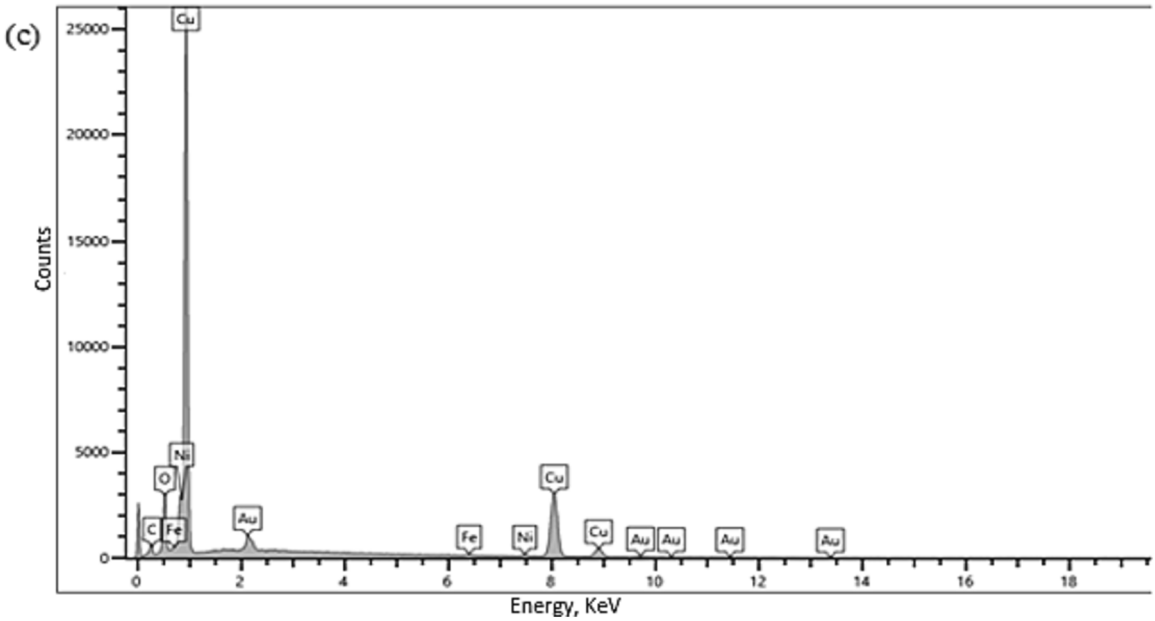


**Fig. 12.** Metallurgical analysis of the external fractured zone (a) morphology of inclusions and EDS mapping points (b) EDS spectrum of the highlighted zones at the edge.

Ziaei et al. [24] observed the same failure pattern for the control valve body of the A216-WCC weld head. The wet, $H_2S$-rich atmosphere was cited as the source of sulphide stress corrosion cracking. Surface pits with corrosion by-products are a defining feature of sulphide-induced SCC. In the present study, the crack branching could be due to the direct contact of the pipe's external surface with $H_2S$ during service at the geothermal power plant.

The EDS mapping of the ruptured pipe in five regions is shown in Fig. 12 (a). Spectrums 8 and 9 were taken in the region containing the cupronickel tube material, while spectrum 11 was obtained in the outer region with corrosion deposits, and spectrums 7 and 10 at the surface of the tube where surface pits, splits, and inclusions are present. Spectrum 9 has a balanced Fe and Mn because it was taken at a region without defects, resembling the standard CuNi strengthening elements. Moreover, it does not have oxygen content to show the absence of oxides from the oxidation reaction. However, high oxygen content in the range of 8.5–10.5 could be seen in spectrums 7, 8, 10, and 11. This indicates the presence of oxides at the tube surface, which penetrated the material to cause degradation. The process of oxidation depletes the iron and manganese strengthening elements in spectrums 7, 8, and 11, where the crack propagates.

The presence of inclusions could be due to Fe and Mn, which reacted with S to form FeS and MnS inclusions, which can cause inclusions at the interface leading to crack initiation when subjected to elevated pressures. Spectrum 11, which contains corrosion residues, has a high iron and oxygen content to indicate the presence of iron oxide that might have been eroded or formed during oxidation. Also, the nickel content is depleted at regions of failure, showing that nickel protects the CuNi pipe from degradation. A similar pattern of oxide formation was observed for EDS mapping of the internal surface of the failed tube and corrosion residues, as shown in Fig. 13. Therefore, it can be concluded that the depletion of essential elements aggravated the prevalence of corrosion because the protective layer was compromised by erosion-wear and $H_2S$ attacks. Table 3 shows the chemical composition of the failed

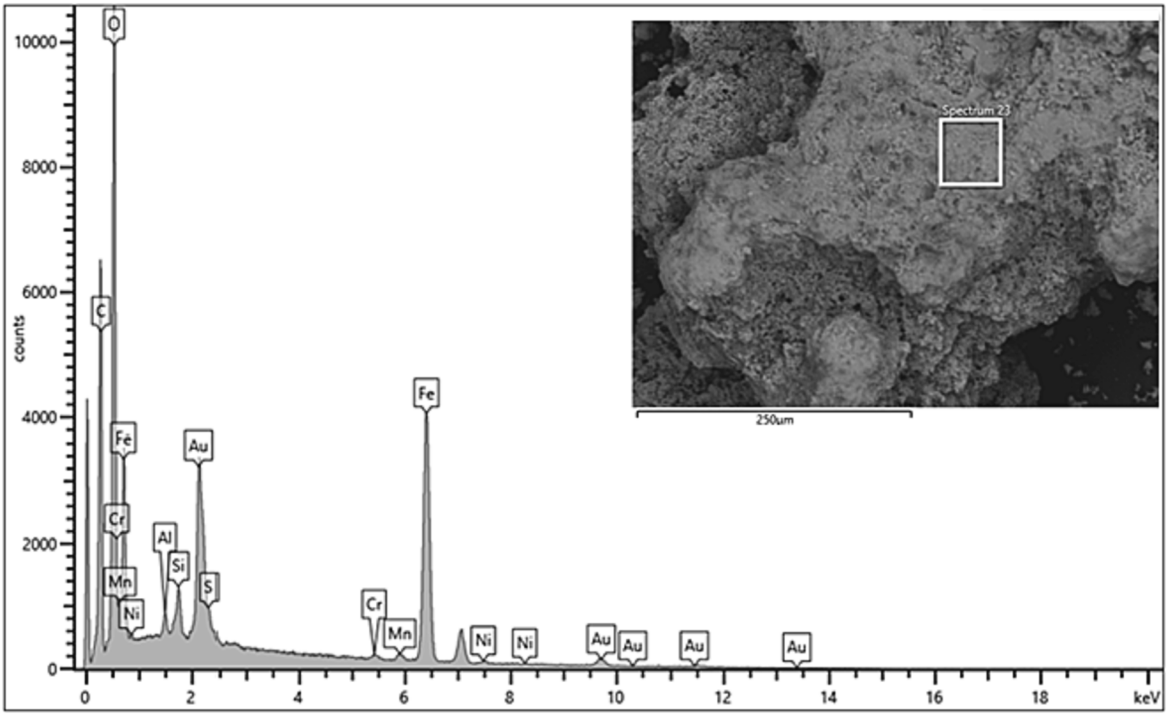


**Fig. 13.** Feature of the corrosion residues and the spectrum of SEM elemental analysis.

**Table 3**
Chemical composition of the exchanger tubes and corrosion residue.

| Element | Cu | Fe | S | Cl | O | Ca | Mn | Si | Al | Ni |
|---|---|---|---|---|---|---|---|---|---|---|
| Corrosion residues | – | 60.28 | 1.24 | – | 33.24 | – | 1.19 | 1.71 | 0.97 | 0.83 |
| Intact (wt.%) | 83.11 | 1.76 | 0.33 | 0.29 | 2.87 | 0.30 | 0.74 | – | – | 10.60 |
| Failed (wt.%) | 89.22 | – | – | – | 9.38 | – | – | – | – | 1.40 |

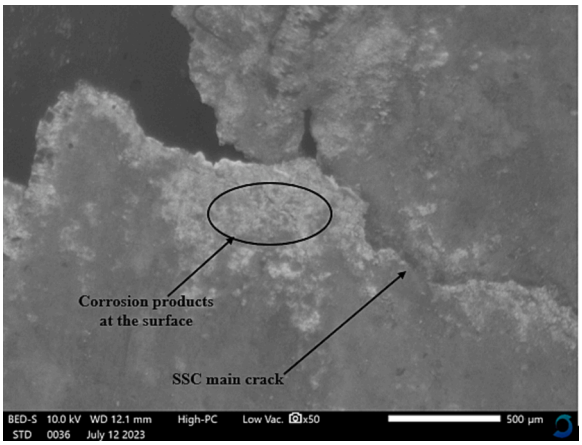


**Fig. 14.** SEM micrographs showing main crack at the surface due to sulfide stress cracking.

and intact tube.

In the geothermal environment, CuNi10Fe interacts with hydrogen sulfide gas to produce corrosion products including metal sulfides (MeS) and atomic hydrogen (H), which combine to generate $H_2$. The created $H_2$ then disperses into the matrix of the material. As a result, the material develops cavities and loses its mechanical strength. These voids can trigger the primary crack propagating

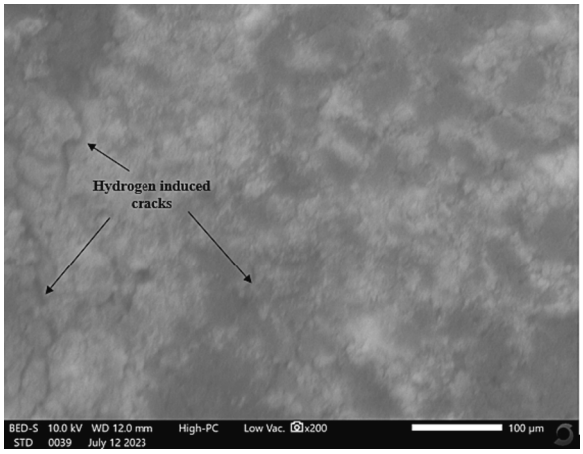


**Fig. 15.** SEM micrographs of hydrogen induced cracks in the failed tube material.

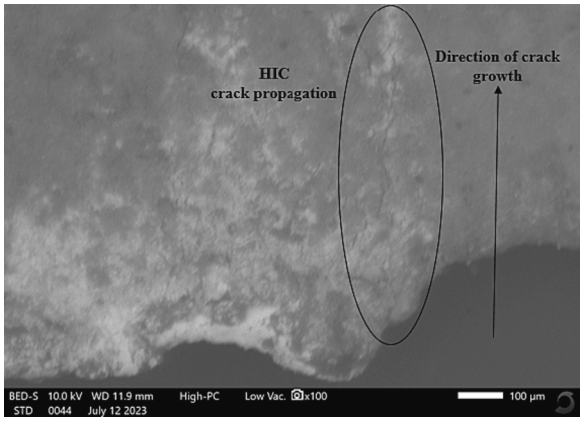


**Fig. 16.** SEM micrographs of the failed tube showing crack propagation.

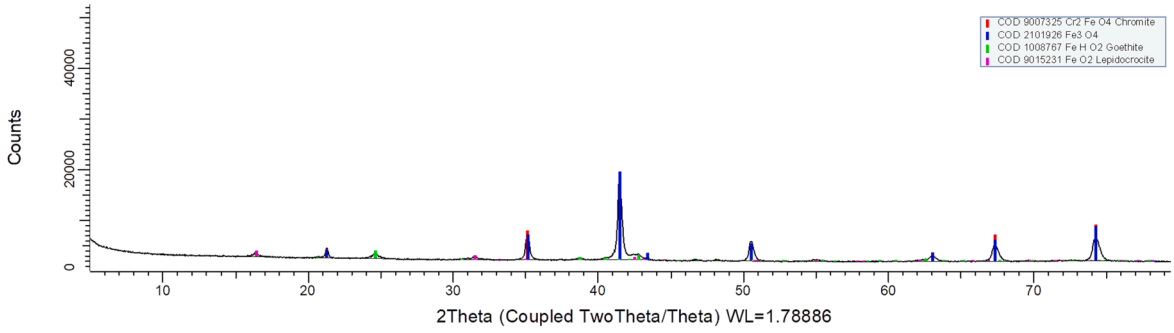


**Fig. 17.** XRD pattern of corrosion residues from CuNi10Fe failed tube.

(hydrogen-induced cracks) and ultimate tube rapture through sulfide stress cracking mechanism when the material is subjected to high fluid pressures, as shown in Fig. 14. Fig. 15 shows the micro-cracks due to hydrogen voids, leading to hydrogen induced cracks. When the material continues being subjected to applied stress during service, the crack propagates, see Fig. 16. This mechanism of degradation has been reported by several researchers [11,25,26] .

### *3.6. X-ray diffraction analysis*

The corrosion residue that was scraped from the heat exchanger is depicted in Fig. 17 using an XRD pattern. The spectrum reveals

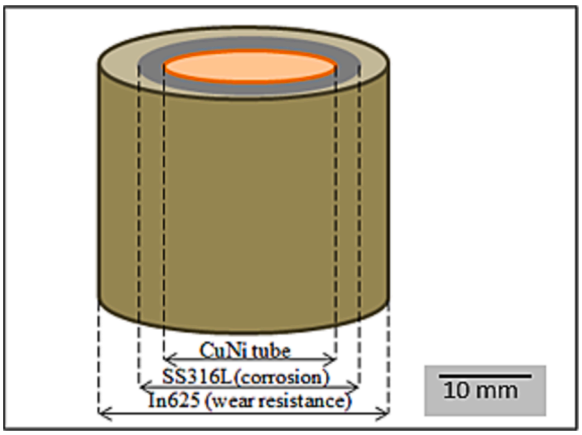


**Fig. 18.** Illustration of SS316L/In625 functionally graded coating on CuNi tube.

the existence of several phases, including magnetite ($Fe_3O_4$), lepidocrocite ($FeO_2$), goethite ($FeHO_2$), and chromium iron oxide ($Cr_2FeO_4$).

Cupronickel pipes benefit from the strengthening elements of iron and manganese. However, the oxidation of iron can form corrosion products that aggravate the corrosion mechanism. According to the findings, the most prevalent oxide that formed as a deposit on the tube surface is iron oxide ($Fe_3O_4$). This suggests that the catalytic reaction at the tube surface caused by the iron oxide deposits developed as a result of oxidation led to pit development at the surface, as shown in Fig. 11. According to Kim et al. [27], the development of goethite, magnetite, and hematite among other corrosion products speeds up corrosion. Results show that the formation of goethite and iron oxide can cause a localized disintegration of the protective layer, which can then result in aggressive pit corrosion, as was the case in the current study.

## 4. Mitigation measures to combat the degradation of heat exchangers

The findings suggest that the heat exchanger's premature failure was caused by inappropriate material choice, poor tube design for the high-pressure application, and hostile operating conditions. Hence, there is a need to redesign the tube to increase thickness which will transform it into a pipe structure that accommodates large applications because tubes are used where small diameters are required. Also, the coating will be applied on the tube outside/external surface. This shall be meant to protect the pipe from hydrogen-induced cracking that was observed to cause failure at the surface, though it emanated from the inside of the tube. Additionally, the surface coating at the outside surface will mitigate wear at the tube entrance, which was reported to be at the tube surface. Therefore, to avoid such shortcomings, careful selection is required to identify a material resistant to sulfur-induced stress corrosion cracking and one that can withstand iron oxidation. This includes materials such as Inconel 625 and stainless steel 316L that have high corrosion resistance and high strength in severe operating conditions. These materials can also be applied as surface coatings to prevent degradation. Functionally graded materials (FGMs) are an emerging class of novel materials that can be used as surface modifiers. They are realized through the combination of materials with different material properties, varied spatially over volume, and custom tailored for a specific function. For instance, an FGM comprising stainless steel 316L/Inconel 625 can be used to improve the corrosion resistance of CuNi10Fe on the tube inside wall by taking advantage of the excellent corrosion resistance of stainless steel 316L, while improving the wear resistance properties on the outside due to the high strength of Inconel 625, as shown in Fig. 18. The findings of this study were used to formulate an experimental work to fabricate a functionally graded SS316L/IN625 material on a copper substrate in the future. This shall comprise the use of the laser cladding technique, followed by heat treatment to reduce the residual stresses generated during manufacturing. In addition, it is necessary to modify the exchanger tubes and employ acrolein to treat hydrogen sulfide in condensate because it is a less expensive approach.

## 5. Conclusion

The evidence collected suggests that the presence of $H_2S$ in the geothermal environment caused hydrogen-induced cracking and sulfide corrosion cracking.

1. High-turbulent fluid pressures eroded the protective cupronickel layer, leading to erosion-wear at the tube opening. The abrasive particles in the fluid aggravated the loss of material and led to material weakness and allowing the diffusion of atomic hydrogen into the material. Proper design consideration of the tube can be employed to accommodate the working fluid pressure.
2. The presence of a wet $H_2S$ environment is the leading environmental factor contributing to tube rupture. This takes place when hydrogen atoms diffuse through into the material, causing the heat exchanger tubes to suffer sulfide stress cracking when subjected

to high pressures. Materials with superior properties including excellent corrosion resistance and wear resistance can be employed as surface modifiers to mitigate hydrogen embrittlement of boiler tubes operating in severe conditions.

3. The presence tensile residual stresses indicate that the stress build-up accumulated along the longitudinal region of the tube. Hence, tube rupture occurred in the same direction as cracks in the microstructure induced by diffusion of hydrogen atoms. Excess residual stresses may be reduced by post-processing such as heat treatment.

## Declaration of Competing Interest

The authors declare the following financial interests/personal relationships which may be considered as potential competing interests: Joseph Bophelo Morake reports financial support was provided by European Union.

## Data availability

No data was used for the research described in the article.

*Acknowledgements*

The authors would like to express profound gratitude to the Kenya Electricity Generating Company (KenGen), particularly Engineer Moses Ikote at Olkaria V geothermal power plant, for assisting with the failed exchanger tube samples. Special recognition goes to Nelson Mandela University (eNtsa) for assisting with the microstructural characterization.

Funding.

This work was supported by the Education for Laser-based Manufacturing (ELbM) consortium, funded by the European Union, grant No. 2019-1973/5 - Project No 614655.

## References

[1] M. Ali, A. Ul-Hamid, L.M. Alhems, A. Saeed, Review of common failures in heat exchangers – Part I: mechanical and elevated temperature failures, Eng. Fail. Anal. 109 (December) (2020), 104396, https://doi.org/10.1016/j.engfailanal.2020.104396.
[2] W. Faes, et al., Corrosion and corrosion prevention in heat exchangers, Corros. Rev. 37 (2) (2019) 131–155, https://doi.org/10.1515/corrrev-2018-0054.
[3] M.R. Khajavi, A.R. Abdolmaleki, N. Adibi, S. Mirfendereski, Failure analysis of bank front boiler tubes, Eng. Fail. Anal. 14 (4) (2007) 731–738, https://doi.org/10.1016/j.engfailanal.2005.10.017.
[4] L. Cozzarini, L. Marsich, C. Schmid, Ant-nest corrosion failure of heat exchangers copper pipes, Eng. Fail. Anal. 109 (March) (2020), 104387, https://doi.org/10.1016/j.engfailanal.2020.104387.
[5] J. Zhou, L. Yan, J. Tang, Z. Sun, L. Ma, Interactive effect of ant nest corrosion and stress corrosion on the failure of copper tubes, Eng. Fail. Anal. 83 (September) (2018) 9–16, https://doi.org/10.1016/j.engfailanal.2017.09.013.
[6] R. Ebara, F. Tanaka, M. Kawasaki, Sulfuric acid dew point corrosion in waste heat boiler tube for copper smelting furnace, Eng. Fail. Anal. 33 (2013) 29–36, https://doi.org/10.1016/j.engfailanal.2013.04.007.
[7] B. Kuźnicka, Erosion–corrosion of heat exchanger tubes, Eng. Fail. Anal. 16 (7) (2009) 2382–2387, https://doi.org/10.1016/j.engfailanal.2009.03.026.
[8] M.M. Lachowicz, A metallographic case study of formicary corrosion in heat exchanger copper tubes, Eng. Fail. Anal. 111 (February) (2020), 104502, https://doi.org/10.1016/j.engfailanal.2020.104502.
[9] R.T. Mousavian, E. Hajjari, D. Ghasemi, M.K. Manesh, K. Ranjbar, Failure analysis of a shell and tube oil cooler, Eng. Fail. Anal. 18 (1) (2011) 202–211, https://doi.org/10.1016/j.engfailanal.2010.08.022.
[10] X. Wang, et al., The influence of copper on the stress corrosion cracking of 304 stainless steel, Appl. Surf. Sci. 478 (January) (2019) 492–498, https://doi.org/10.1016/j.apsusc.2019.01.291.
[11] M.A. Mohtadi-Bonab, Effects of different parameters on initiation and propagation of stress corrosion cracks in pipeline steels: a review, Metals (Basel) 9 (5) (2019) 1–18, https://doi.org/10.3390/met9050590.
[12] Z. Wang, H. Lu, J. Cai, L. Wu, K. Luo, J. Lu, Improvement mechanism in stress corrosion resistance of the X70 pipeline steel in hydrogen sulfide solution by massive laser shock peening treatment, Corros. Sci. 201 (2022), 110293, https://doi.org/10.1016/j.corsci.2022.110293.
[13] A. Usman, A.N. Khan, Failure analysis of heat exchanger tubes, Eng. Fail. Anal. 15 (1–2) (2008) 118–128, https://doi.org/10.1016/j.engfailanal.2006.11.051.
[14] H. Miyamoto, D. Saburi, H. Fujiwara, A microstructural aspect of intergranular stress corrosion cracking of semi-hard U-bend tubes of commercially pure copper in cooling systems, Eng. Fail. Anal. 26 (2012) 108–119, https://doi.org/10.1016/j.engfailanal.2012.07.006.
[15] S. Xu, C. Wang, W. Wang, Failure analysis of stress corrosion cracking in heat exchanger tubes during start-up operation, Eng. Fail. Anal. 51 (2015) 1–8, https://doi.org/10.1016/j.engfailanal.2015.02.005.
[16] K. Chandra, V. Kain, P.S. Shetty, R. Kishan, Failure analysis of copper tube used in a refrigerating plant, Eng. Fail. Anal. 37 (2014) 1–11, https://doi.org/10.1016/j.engfailanal.2013.11.014.
[17] K. Li, Y. Zeng, J.-L. Luo, Influence of H2S on the general corrosion and sulfide stress cracking of pipelines steels for supercritical {CO}2 transportation, Corros. Sci. 190 (2021), 109639, https://doi.org/10.1016/j.corsci.2021.109639.
[18] K. Jaelani, K. Kusmono, P. Utami, R. Budiarto, Corrosion in geothermal facilities: their causes, effects, mitigation, and worldwide cases, AIP Conf. Proc. 2338 (November) (2021), https://doi.org/10.1063/5.0066755.
[19] Y.H. Chan, et al., A state-of-the-art review on capture and separation of hazardous hydrogen sulfide (H2S): recent advances, challenges and outlook, Environ. Pollut. 314 (2022), 120219, https://doi.org/10.1016/j.envpol.2022.120219.
[20] C.D.S. Tuck, R. Emea, Corrosion of Copper and Its Alloys $, June 2015, 2016, doi: 10.1016/B978-0-12-803581-8.01634-9.
[21] J.S. Corte, J.M.A. Rebello, M.C.L. Areiza, S.S.M. Tavares, M.D. Araujo, Failure analysis of AISI 321 tubes of heat exchanger, Eng. Fail. Anal. 56 (2015) 170–176, https://doi.org/10.1016/j.engfailanal.2015.03.008.
[23] X. Yang, M. Liu, Z. Liu, C. Du, X. Li, Failure analysis of a 304 stainless steel heat exchanger in liquid sulfur recovery units, Eng. Fail. Anal. 116 (July) (2020), 104729, https://doi.org/10.1016/j.engfailanal.2020.104729.
[24] S.M.R. Ziaei, A.H. Kokabi, Case Studies in Engineering Failure Analysis Sulfide stress corrosion cracking and hydrogen induced cracking of A216-WCC wellhead flow control valve body, Biochem. Pharmacol. 1 (3) (2013) 223–234, https://doi.org/10.1016/j.csefa.2013.08.001.

[25] M.S. Khoma, K.B. Vasyliv, M.R. Chuchman, Influence of the hydrogen sulfide concentration on the corrosion and hydrogenation of pipe steels (a survey), Mater. Sci. 57 (3) (2021) 308–318, https://doi.org/10.1007/s11003-021-00546-x.
[26] B. Wang, L. Ouyang, J. Xu, P. Huang, E. Liu, B. Yang, Study on stress corrosion cracking behavior of Incoloy825/X65 bimetallic composite pipe welded joint in wet hydrogen sulfide environment, Metals (Basel) 12(4) (2022), doi: 10.3390/met12040632.
[27] H. Chae, et al., Stress corrosion cracking of a copper pipe in a heating water supply system, Met. Mater. Int. 26 (7) (2020) 989–997, https://doi.org/10.1007/s12540-019-00386-0.